American Mineralogist, Volume 77, pages 704–712, 1992

Investigation of cation order in $MgSiO_3$-rich garnet using ^{29}Si and ^{27}Al MAS NMR spectroscopy

Brian L. Phillips,* David A. Howell, R. James Kirkpatrick**
Department of Geology, University of Illinois, Urbana, Illinois 61801, U.S.A.
Tibor Gasparik
Department of Earth and Space Sciences, State University of New York at Stony Brook, Stony Brook, New York 11794, U.S.A.

Abstract

Cation order among the octahedral sites of three polycrystalline ^{29}Si-enriched garnets on the enstatite-pyrope join (En_{100}, $En_{80}Py_{20}$, and $En_{50}Py_{50}$) has been examined using ^{29}Si and ^{27}Al MAS NMR spectroscopy. These samples were synthesized at 17.7 GPa and 2000 °C. All three samples yielded ^{29}Si NMR peaks in the chemical shift range of -68 to -90 ppm, caused by $^{[4]}Si$, and a peak between -195.6 and -197.5 ppm, caused by $^{[6]}Si$. The $^{[4]}Si/^{[6]}Si$ ratios are consistent with the compositions, with the assumption that all Al is octahedrally coordinated, as indicated by the ^{27}Al NMR spectra of the samples. The tetragonal $MgSiO_3$ end-member garnet (En_{100}, majorite) yields a peak for each of the three tetrahedral sites plus several smaller $^{[4]}Si$ peaks caused by some Mg,Si disorder on the next-nearest-neighbor (NNN) octahedral sites. The occupancies of the two nonequivalent octahedral sites (Oc1 and Oc2) derived from the ^{29}Si NMR spectrum are 0.88(3) Mg + 0.12(3) Si for Oc1 and 0.12(3) Mg + 0.88(3) Si for Oc2 and are similar to those found previously by single-crystal X-ray diffraction. For the cubic $En_{80}Py_{20}$ and $En_{50}Py_{50}$, the $^{[4]}Si$ portions of the NMR spectra can be simulated with intensities similar to those of a random distribution of Mg, Al, and Si over the octahedral sites, suggesting that these samples contain little short-range octahedral Mg,Al,Si order.

The changes in the ^{29}Si chemical shifts for $^{[4]}Si$ with substitution of Mg for Si on the NNN octahedral sites are pairwise rather than directly additive, in contrast to the effect of Si,Al substitution on ^{29}Si chemical shifts in framework silicates. The pairwise additivity constants are $\eta_{Mg\text{-}Si} = -0.8$ ppm and $\eta_{Si\text{-}Si} = -3.4$ ppm, relative to $\eta_{Mg\text{-}Mg} \equiv 0.0$ for En_{100}.

Introduction

Many of the current petrological models of the Earth's lower upper-mantle and transition zones include the high-pressure transformation of pyroxene to the mineral majorite, which has the garnet structure. Majorite is an unusual garnet because it contains $^{[6]}Si$ and because the enstatite-composition end-member has tetragonal rather than cubic symmetry at ambient conditions. Garnets with compositions between $MgSiO_3$ (En) and $Mg_3Al_2Si_3O_{12}$ (Py) contain Si, Mg, and Al in sixfold coordination, which may be disordered over the octahedral sites in the crystal. The distribution of the octahedral cations affects the thermodynamic properties of majorite caused by increased configurational entropy and the possibility of order-disorder phase transitions (Akaogi and Akimoto, 1977; Akaogi et al., 1987; Hatch and Ghose, 1989). In this study we present a ^{29}Si NMR study of three ^{29}Si-enriched garnets along the enstatite-pyrope join (En_{100}, $En_{80}Py_{20}$, and $En_{50}Py_{50}$). For the enstatite-composition end-member the resolution of the peaks allows quantitative determination of the occupancies of the two octahedral sites and comparison to those derived from single-crystal XRD (Angel et al., 1989).

Experimental methods

Sample description

Garnets with the compositions En_{100}, $En_{80}Py_{20}$, and $En_{50}Py_{50}$ were synthesized from glass at 17.7 GPa and 2000 °C with the uniaxial-split sphere apparatus (USSA-2000) at the Stony Brook High-Pressure Laboratory (Remsberg et al., 1988). The glasses were synthesized by melting the required amounts of 95% ^{29}Si-enriched SiO_2 (Oak Ridge National Laboratory) and 99.999% pure Al_2O_3 and MgO (Aldrich) in Pt boats at 1500 °C for 3 h. The material was then ground and remelted to ensure homogeneity. Optical examination of the glasses revealed no crystalline material or heterogeneities. The garnet samples were 4–8 mg each and polycrystalline, with an average grain size of 3–10 μm.

* Present address: L-219, Lawrence Livermore National Laboratory, P.O. Box 808, Livermore, California 94550, U.S.A.
** Present address: Department of Metallurgy, Mechanics, and Materials Science, Michigan State University, East Lansing, Michigan 48824, U.S.A.

0003–004X/92/0708–0704$02.00

TABLE 1. Chemical analysis of garnet samples

Wt%	En_{100}	$En_{80}Py_{20}$	$En_{50}Py_{50}$
SiO_2	59.58(35)	57.31(46)	52.19(11)
Al_2O_3	0.26(10)	4.92(06)	12.79(06)
MgO	40.32(30)	37.88(54)	35.40(12)
Total	100.16(33)	100.11(42)	100.38(15)

Note: Average of seven electron microprobe analyses. Accelerating voltage was 15 kV with a beam current of 15 nA. The beam diameter was 10 μm. Recalculated formulas of En_{100}, $En_{80}Py_{20}$, $En_{50}Py_{50}$ based on 12 O atoms: $Mg_{4.04}Si_{3.96}O_{12}$, $Mg_{3.81}Al_{0.40}Si_{3.79}O_{12}$, $Mg_{3.54}Al_{1.00}Si_{3.46}O_{12}$.

A small fraction of each sample was powdered and analyzed by powder X-ray diffraction. The En_{100} sample yielded diffraction peaks in agreement with previous powder diffraction results for $MgSiO_3$ garnet (Kato and Kumazawa, 1985; Sawamoto, 1987). The intermediate compositions $En_{80}Py_{20}$ and $En_{50}Py_{50}$ yielded diffraction patterns similar to a synthetic pyrope garnet. Corundum was detected in the powdered En_{100} sample and is probably from the cell assembly used in the split-sphere apparatus. No other phases were detected in any of the samples. Electron microprobe analysis shows that the measured compositions are the nominal compositions within analytical error (Table 1).

The end-member pyrope sample was synthesized from an oxide mixture with 10 mol% excess silica at 1000 °C with P_{H_2O} = 23.5 kbar (O'Neill et al., 1991). Its composition from electron microprobe analysis is $Mg_{3.03}Al_{1.97}Si_{2.99}O_{12}$. Powder XRD of the pyrope yielded a lattice parameter a = 11.457(2) Å.

NMR spectroscopy

The ^{29}Si NMR spectra were obtained at 71 MHz at room temperature using a home-built spectrometer that consists of an 8.45-T superconducting magnet (Oxford Instruments, Oxford, U.K.) and a Nicolet (Madison, Wisconsin) model 1280 computer and pulse programmer. The samples were spun at 3–4 kHz in a Doty Scientific (Columbia, South Carolina) MAS probe using a sapphire rotor with a 7-mm od. The pieces of garnet (4–8 mg total) were wrapped in Teflon tape and then packed with powdered NaCl into the rotor. The excitation pulse was 5 μs (π/4), and the recycle delay was 10 s. The spin-lattice relaxation time for each of the main peaks for the En_{100} sample was 3 ± 0.5 s. The relative peak intensities did not change with a change in the delay from 10 to 60 s, indicating that the peak areas may be used quantitatively to measure populations. Between 1000 and 2000 scans were required for a sufficient signal-to-noise ratio. The chemical shifts reported in Table 2 are relative to external tetramethylsilane (TMS). The intensities of the observed ^{29}Si NMR peaks were obtained by fitting the spectra to a sum of Lorentzian and Gaussian curves using a computer program that minimizes χ^2 by varying the position, height, and full width at half height (FWHH). This program is based on a Levenberg-Marquardt algorithm (Press et al., 1986).

The ^{27}Al spectra were obtained at 130 MHz using a similar spectrometer with an 11.7-T superconducting magnet (Oxford Instruments). The samples were spun in zirconia rotors with a 5-mm od at 8–9 kHz with a Doty Scientific MAS probe. The excitation pulse was 2 μs (π/6), and the recycle delay was 2 s. Between 300 and 400 scans were required for a sufficient signal-to-noise ratio. The ^{27}Al chemical shifts (Table 2) are reported relative to external 0.1 M $Al(NO_3)_3$ solution.

TABLE 2. The ^{29}Si and ^{27}Al NMR chemical shifts (in ppm) and fitted intensities for $^{[4]}Si$ of garnet samples

Sample	Site	^{29}Si δ	$^{[4]}Si$ relative intensity	^{27}Al δ
En_{100}	T1(4Mg 0Si)	−68.1	0.126	
	T1(3Mg 1Si) + T3(3Mg 1Si)	−70.7	0.087	
	T3(2Mg 2Si)	−74.5	0.578	
	T1(1Mg 3Si)	−79.9	0.024	
	T3(1Mg 3Si)	−82.0	0.054	
	T2(1Mg 3Si)	−83.8	0.005	
	T3(0Mg 4Si)	−88.5	0.024	
	T2(0Mg 4Si)	−90.2	0.097	
	$^{[4]}Si$ center of gravity	−75.8		
	$^{[6]}Si$ center of gravity	−196.8		
	$^{[6]}Si$	−197.5		
	$^{[6]}Al$			13.5, 1.2
$En_{80}Py_{20}$	$^{[4]}Si$ center of gravity	−74.5		
	$^{[6]}Si$	−195.8		
	$^{[6]}Al$			1.3
$En_{50}Py_{50}$	$^{[4]}Si$ center of gravity	−74.0		
	$^{[6]}Si$	−195.6		
	$^{[6]}Al$			2.1
Py_{100}	$^{[4]}Si$	−72.0		
	$^{[6]}Al$			2.4

Note: Estimated uncertainties are ±0.1 ppm for chemical shifts and ±0.01 for fitted intensities; ^{27}Al δ are peak positions.

RESULTS

The ^{29}Si MAS NMR spectrum of the En_{100} sample contains three large peaks in the chemical shift range for $^{[4]}Si$ (−68.1, −74.5, and −90.2 ppm), five smaller peaks or shoulders in this range, and a large peak at −197.5 ppm in the range for $^{[6]}Si$ (Figs. 1, 2, Table 2). The chemical shifts of the three main $^{[4]}Si$ peaks and the $^{[6]}Si$ peak are in excellent agreement with values given by Stebbins and Kanzaki (1991). The ratio of the integrated intensities for $^{[4]}Si$ and $^{[6]}Si$ is 3/1, as expected for stoichiometric tetragonal $MgSiO_3$ garnet (Angel et al., 1989). The −197.5-ppm chemical shift for $^{[6]}Si$ in majorite is more shielded than that for $^{[6]}Si$ in stishovite (−191.3 ppm; Smith and Blackwell, 1983; Grimmer et al., 1986) and $MgSiO_3$ perovskite (−191.7 ppm; Kirkpatrick et al., 1991). This peak is also broader (FWHH = 1.3 ppm) than for these phases (stishovite, FWHH = 0.4 ppm; perovskite, FWHH = 0.2 ppm) and is slightly asymmetric to less negative chemical shifts (higher frequency).

The ^{29}Si NMR spectra of the intermediate composition garnets (Figs. 1, 2) contain broader, less well-resolved peaks in the range for $^{[4]}Si$ and peaks for $^{[6]}Si$ at −195.8 ppm ($En_{80}Py_{20}$) and −195.6 ppm ($En_{50}Py_{50}$). The range of

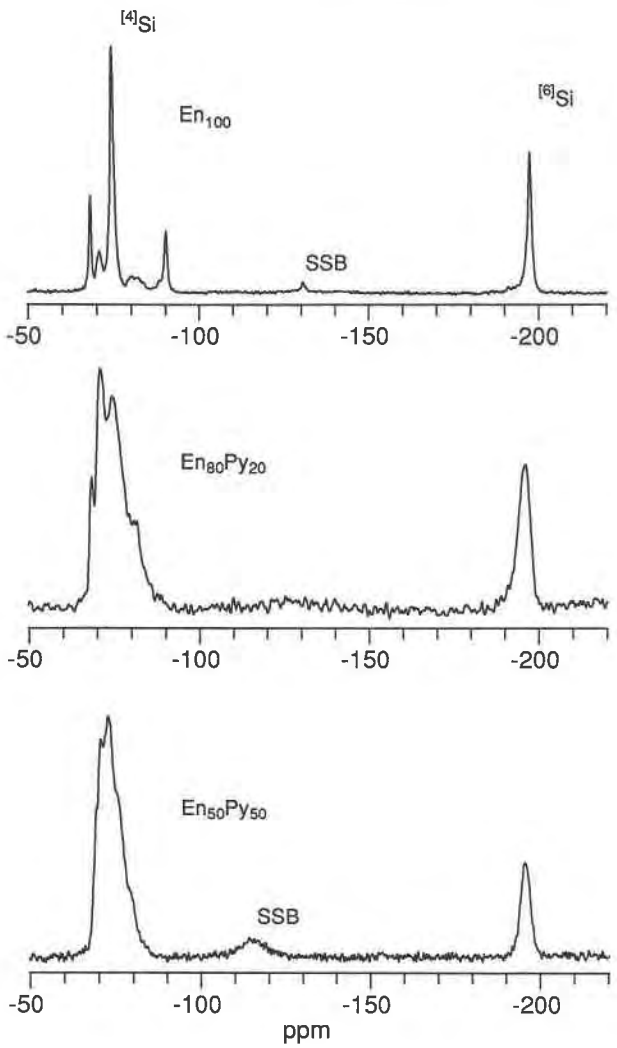

Fig. 1. The ^{29}Si MAS NMR spectra of En_{100}, $En_{80}Py_{20}$, and $En_{50}Py_{50}$ garnets, showing both $^{[4]}Si$ and $^{[6]}Si$ peaks. The chemical shifts are reported relative to tetramethylsilane (TMS).

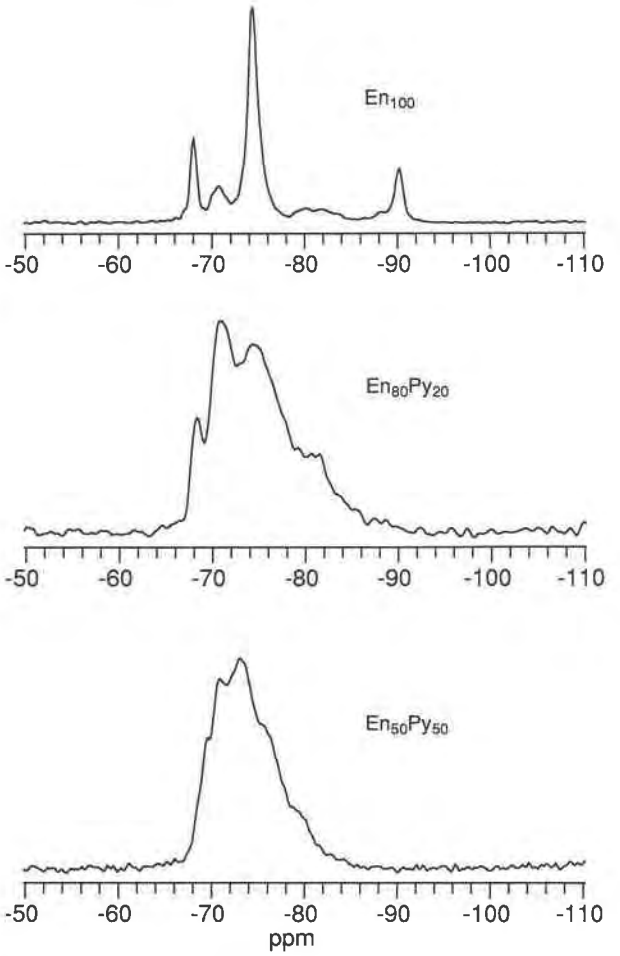

Fig. 2. Expanded ^{29}Si MAS NMR spectra showing the $^{[4]}Si$ region for En_{100}, $En_{80}Py_{20}$, and $En_{50}Py_{50}$ garnets. The three well-defined peaks at -68.1 ppm, -74.5 ppm, -90.2 ppm for En_{100} are assigned to the T1(4Mg 0Si), T3(2Mg 2Si), and T2(0Mg 4Si) sites, respectively. The smaller, less resolved peaks are due to sites with 3Mg + 1Si and 1Mg + 3Si NNN resulting from Si,Mg disorder on the octahedral sites. Peaks for intermediate compositions are broader due to the presence of 15 possible sites as a result of Mg,Al,Si disorder on the octahedral NNN to the $^{[4]}Si$.

chemical shifts for $^{[4]}Si$ in these samples is similar to that for En_{100} garnet (about -68 to -90 ppm for $En_{80}Py_{20}$ and -68 to -86 ppm for $En_{50}Py_{50}$). However, neither has a large peak near -90 ppm. Rather, the intensity in the central part of this chemical shift range (about -70 to -82 or -86 ppm) is greater than that for the En_{100} sample. The peaks for $^{[6]}Si$ in the $En_{80}Py_{20}$ and $En_{50}Py_{50}$ samples are at slightly higher frequencies than the $^{[6]}Si$ peak of En_{100} and are approximately three times as broad (FWHH = 4.2 and 3.4 ppm, respectively). The ratios of the intensities for $^{[4]}Si$ and $^{[6]}Si$ are 3.65 for $En_{80}Py_{20}$ and 6.03 for $En_{50}Py_{50}$. These values are within experimental uncertainty of the values expected, with the assumption that all Al is $^{[6]}Al$ (3.75 and 6.00).

The ^{27}Al MAS NMR spectra of our En-Py garnets contain a signal in the chemical shift range for $^{[6]}Al$ (Fig. 3). No signal for $^{[4]}Al$ was detected in the ^{27}Al MAS NMR spectra, in agreement with the results of McMillan et al. (1989).

The ^{27}Al MAS NMR spectra of the $En_{80}Py_{20}$ and $En_{50}Py_{50}$ samples contain one peak with maxima at 1.3 and 2.1 ppm, respectively. Most of the Al in the $MgSiO_3$ garnet sample is from unreacted corundum that probably entered the capsule from the cell assembly during synthesis in the split-sphere apparatus. The breadth (FWHH = 6.5 ppm) and peak maximum (13.5 ppm) of the main peak are similar to those of corundum (Dupree et al., 1988). The ^{27}Al NMR spectrum of the En_{100} sample also contains a small peak (0.2%) at about 1 ppm that may be due to the garnet phase, which would indicate that a small amount of Al entered the garnet during synthesis. We do not expect this amount of Al to have significantly affected the ^{29}Si results discussed below.

The synthetic pyrope sample yielded a single ^{29}Si MAS NMR peak at -72.0 ppm (spectrum not shown) and a

single ^{27}Al MAS NMR peak at 2.4 ppm due to $^{[6]}Al$ (Fig. 3). Thus, the ^{27}Al peak maximum of garnet becomes more positive with increasing Py component, as previously observed by McMillan et al. (1989).

Discussion

$MgSiO_3$ garnet

Peak assignments. We base the assignment of the $^{[4]}Si$ NMR peaks for $MgSiO_3$ (En_{100}) garnet on the average structure as determined from single-crystal X-ray diffraction results (Angel et al., 1989) and on the well-known relationship between increasing bond strength of the NNN cations to Si and increased shielding at Si (Smith et al., 1983; Sherriff and Grundy, 1988). In this case, the ^{29}Si chemical shifts of $^{[4]}Si$ become more shielded (more negative) with substitution of $^{[6]}Si$ NNN for $^{[6]}Mg$ NNN. The 1-bar, room-temperature structure of En_{100} garnet (space group $I4_1/a$) contains three tetrahedral sites (T1, T2, and T3) with multiplicities 4, 4, and 16, respectively, and two octahedral sites (Oc1 and Oc2). T1 shares all four O atoms with Oc1, T2 shares all four O atoms with Oc2, and T3 shares two O atoms with Oc1 and two with Oc2. The refined occupancies of the octahedral sites based on X-ray diffraction results are 0.80 Mg + 0.20 Si for Oc1 and 0.20 Mg + 0.80 Si for Oc2 (Angel et al., 1989).

Thus, the peak at −68.1 ppm is readily assigned to Si on T1 with four $^{[6]}Mg$ NNN [e.g., T1(4Mg)], that at −74.5 ppm to Si on T3 with two $^{[6]}Mg$ and two $^{[6]}Si$ NNN [T3(2Mg 2Si)], and that at −90.2 ppm to Si on T2 with four $^{[6]}Si$ NNN [T2(4Si)]. These assignments agree with both the site multiplicities and known NNN effects on ^{29}Si chemical shifts.

We attribute the smaller $^{[4]}Si$ peaks to Si on T1, T2, and T3 with other than these ideal numbers of $^{[6]}Mg$ and $^{[6]}Si$ NNNs, because of Mg,Si disorder on the octahedral sites. The small peak at −70.7 ppm is readily attributable to T(3Mg 1Si) (crystallographic T sites not resolved). The group of peaks at −79.9, −82.0, and −83.8 ppm is likely from T(1Mg 3Si), probably on all three crystallographic T sites, although we have no way to assign them unambiguously. The small peak at −88.5 ppm is probably due to T3(4Si). The presence of this latter peak indicates that the peak at −68.1 ppm may include some intensity from Si on T3 with four $^{[6]}Mg$ NNN [i.e., T3(4Mg)].

The $^{[6]}Mg/^{[6]}Si$ ratio computed from the relative intensities of the $^{[4]}Si$ peaks and our assignment of these peaks (Table 2) equals that expected from the composition, indicating that all of the peaks in the region for $^{[4]}Si$ are probably caused by the garnet and not some impurity phase. From the ^{29}Si NMR spectrum, the $^{[6]}Mg/^{[6]}Si$ ratio is given by

$$^{[6]}Mg/^{[6]}Si = \frac{\sum_{n=0}^{4} n \cdot I_{n\mathrm{Mg}}}{4 - \sum_{n=0}^{4} n \cdot I_{n\mathrm{Mg}}} \quad (1)$$

where $I_{n\mathrm{Mg}}$ is the fraction of the $^{[4]}Si$ intensity assigned to Si having n $^{[6]}Mg$ NNN. Using the assignments given above

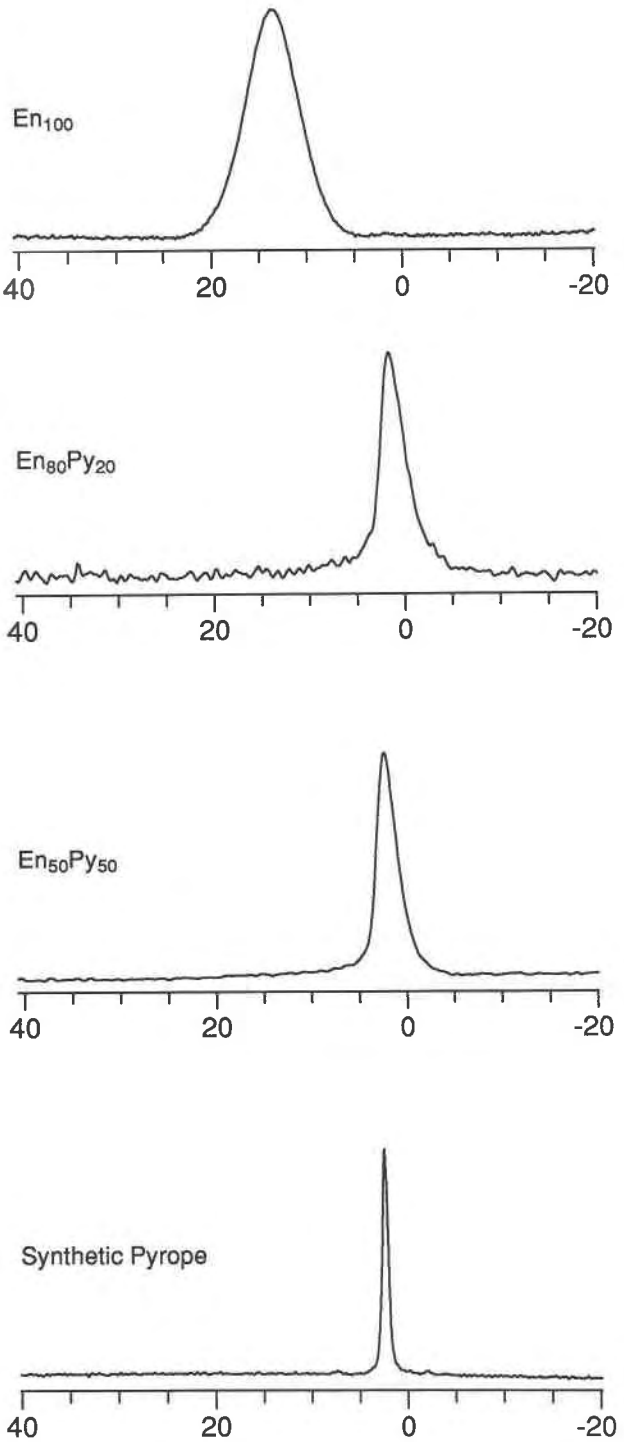

Fig. 3. Four ^{27}Al MAS NMR spectra showing $^{[6]}Al$ in En_{100}, $En_{80}Py_{20}$, and $En_{50}Py_{50}$ garnets and the synthetic pyrope sample. The broad peak at 13.5 ppm for the En_{100} sample indicates that the Al in the microprobe analysis arises from corundum. As the pyrope component increases in the intermediate compositions ($En_{80}Py_{20}$ and $En_{50}Py_{50}$), the Al peak maximum shifts progressively toward that of the synthetic pyrope, and the peaks become more narrow.

and fitted intensities (Table 2) gives $^{[6]}Mg/^{[6]}Si = 1.00$, in agreement with the composition. Assignment of the $^{[4]}Si$ peaks in a significantly different manner would cause the calculated ratio of $^{[6]}Mg/^{[6]}Si$ to differ from one.

The $^{[6]}Mg,^{[6]}Si$ order. The relative intensities of the peaks due to $^{[4]}Si$ allow us to determine precisely the extent of long-range $^{[6]}Mg,^{[6]}Si$ order and show that, for our sample, Oc1 contains on average 0.88(3) Mg + 0.12(3) Si and Oc2 contains 0.12(3) Mg + 0.88(3) Si. These values correspond to slightly more ordering than those observed by Angel et al. (1989) on the basis of XRD data (0.80 ± 0.06) but agree within analytical uncertainty. In addition, there appears to be some additional short-range order that leads to a larger population of T(2Mg 2Si) sites and fewer T(1Mg 3Si) and T(3Mg 1Si) sites than those calculated for a random distribution of local configurations.

We estimated the occupancies of the octahedral sites by comparing the observed intensity of the peak assigned to T2(4Si) (−90.2 ppm) with populations calculated from limiting models for the short-range $^{[6]}Si,^{[6]}Mg$ order. We used the T2(4Si) peak because the chemical shift dispersion is greater there than near the T1(4Mg) peak, allowing the T2(4Si) and T3(4Si) peaks to be resolved. Also, the peak assigned to T1(4Mg) (−68.1 ppm) might contain intensity from T3(4Mg) sites.

To perform this calculation, we must distinguish long-range order, i.e., the average occupancies of the octahedral sites, from short-range order. Short-range order includes the relative populations of the various local configurations of octahedral cations around each tetrahedral site [e.g., T1(4Mg), T1(3Mg 1Si), etc.]. XRD techniques can determine only the average site occupancies because of the long correlation length for coherent scattering. The intensities of the individual $^{[4]}Si$ NMR peaks, however, depend on both the average distribution of Si and Mg on the crystallographic octahedral sites and how these octahedrally coordinated cations are arranged locally about each T site.

For a given population of T2(4Si) sites, two limiting short-range ordering models bracket the possible range of average octahedral site occupancies. One assumes no short-range $^{[6]}Si,^{[6]}Mg$ order; the probability that a particular Oc2 site is occupied by Mg does not depend on the occupancy of adjacent octahedral sites. The second assumes that the Mg atoms on Oc2 are distributed evenly such that only one occurs about any T2, producing only T2(4Si) and T2(3Si) environments [i.e., no Oc2(Mg)-O-T2-O-Oc2(Mg) linkages].

In the model assuming no short-range $^{[6]}Si,^{[6]}Mg$ order, the fraction of Oc2 occupied by Si ($f_{Oc2(Si)}$) is given by the binomial distribution

$$f_{Oc2(Si)} = (6I_{T2(4Si)})^{1/4}. \quad (2)$$

For $I_{T2(4Si)} = 0.097(10)$ (Table 2), Equation 2 gives $f_{Si(Oc2)} = 0.87(2)$. In the model that assumes an even distribution of Mg on Oc2,

$$f_{Oc2(Si)} = \tfrac{1}{4}(6I_{T2(4Si)} + 3.0). \quad (3)$$

For $I_{T2(4Si)} = 0.097(10)$, this model gives $f_{Oc2(Si)} = 0.89(2)$. The small range of values for $f_{Oc2(Si)}$ bracketed by these two limiting models indicates that the intensity of the T2(4Si) peak is sensitive to the average occupancies of the octahedral sites, but not to the degree of short-range $^{[6]}Mg,^{[6]}Si$ order.

An average of the above values of $f_{Oc2(Si)}$ for our En_{100} garnet gives average site occupancies 0.88(3) Mg + 0.12(3) Si for Oc1 and 0.12(3) Mg + 0.88(3) Si for Oc2. These values for the octahedral site occupancies agree, within analytical uncertainty, with the previous X-ray diffraction results [0.80(6); Angel et al., 1989] but also support the suggestion of Angel et al., based on the $^{[6]}M$-O bond lengths, that the actual degree of order is slightly higher than given by the refined occupancies. However, the degree of $^{[6]}Mg,^{[6]}Si$ order may depend on synthesis conditions and quench rate, and thus there might be some difference between our sample and theirs.

The peak for $^{[6]}Si$ in the ^{29}Si spectrum of the En_{100} sample supports a distribution of 0.88 $^{[6]}Si$ in Oc2 and 0.12 in Oc1. Approximately 10% of the $^{[6]}Si$ intensity is contained in a relatively broad tail extending from the narrow central portion of the peak toward less negative chemical shifts. The tail is toward the $^{[6]}Si$ chemical shifts observed for the intermediate compositions and is probably due to $^{[6]}Si$ on Oc1. Structural distortions about the disordered Si on Oc1 probably result in a distribution of local configurations and chemical shifts, which precludes resolution of a separate peak.

Finally, we note that the average site occupancies do not describe completely the ordering of the octahedral cations. The presence of additional short-range order in the local configurations of the octahedral cations is indicated by the departure of the intensities of the T(2Mg 2Si), T(3Mg 1Si), and T(1Mg 3Si) peaks from those computed for a random distribution (Table 3). From the average site occupancies determined above and a random distribution of local configurations, the populations for T(3Mg 1Si), T(2Mg 2Si), and T(1Mg 3Si), summed over the crystallographic sites, would be 0.167, 0.452, and 0.167, respectively (Table 3). The corresponding observed values, 0.087(10), 0.578 (10), and 0.083(10), are significantly different and indicate a preference for T(2Mg 2Si) environments over T(3Mg 1Si) + T(1Mg 3Si) environments. This additional short-range order decreases the configurational entropy from what one would calculate on the basis of the site occupancies alone.

Pairwise additivity of ^{29}Si chemical shifts. The large spread of ^{29}Si chemical shifts (δ) for $^{[4]}Si$ in En_{100} garnet, −68.1 to −90.2 ppm, and the nonlinear change of δ with the number of $^{[6]}Mg$ NNN are somewhat surprising and cannot be explained on the basis of previous correlations of ^{29}Si chemical shift and crystal structure. The variation of δ with occupancy of the NNN octahedral sites, however, is described well by a pairwise rule for adding the effects of $^{[6]}Mg$ and $^{[6]}Si$ on the $^{[4]}Si$ δ that was developed originally to explain substituent effects on NMR chemical shifts in solution. Because pairwise additivity of δ has not

TABLE 3. Estimated chemical shifts, fitted intensities, and calculated populations of the 15 possible [4]Si NNN environments in En-Py garnets

Site	Estimated ^{29}Si δ (ppm)	Relative populations					
		En_{100}		$En_{80}Py_{20}$		$En_{50}Py_{50}$	
		Fit*	rd**	Fit	rd	Fit	rd
4Mg	−68.1	0.126	0.107	0.059	0.026	—	0.004
3Mg1Al	−68.7			0.015	0.051	0.042	0.031
2Mg2Al	−69.5			0.018	0.038	0.060	0.094
3Mg1Si	−70.5	0.087	0.167	a	0.102	a	0.016
				0.167		0.129	
1Mg3Al	−70.7			a	0.013	a	0.125
2Mg1Al1Si	−71.9			b	0.154	b	0.094
				0.100		0.172	
4Al	−72.0			b	0.002	b	0.063
1Mg2Al1Si	−73.5			0.127	0.077	0.190	0.188
2Mg2Si	−74.8	0.578	0.452	0.126	0.154	0.024	0.023
3Al1Si	−75.3			0.013	0.013	0.139	0.125
1Mg1Al2Si	−76.8			0.164	0.154	0.116	0.094
2Al2Si	−79.1			0.036	0.038	0.085	0.094
1Mg3Si	−80.7	0.083	0.167	0.106	0.102	0.028	0.016
1Al3Si	−83.5			0.050	0.051	0.017	0.031
4Si	−88.5	0.121	0.107	0.019	0.026	—	0.004

* Uncertainties are approximately ±0.01 for En_{100}; fitted values for $En_{80}Py_{20}$ and $En_{50}Py_{50}$ are only approximate and are sensitive to fixed values of δ and peak width.

** Calculated populations assuming a random distribution of (Mg,Al,Si) on the octahedral sites; a and b indicate sites that have nearly the same chemical shift and have been combined into one peak. Random distribution = rd.

been observed previously in geologically important phases, we briefly describe it below.

Previous correlations of ^{29}Si δ, successful for a wide range of silicate structures, fail to reproduce the values observed for the tetrahedral crystallographic sites in En_{100} garnet. The method of Janes and Oldfield (1985), based on a sum of group electronegativities, gives values of −61.9, −66.7, and −71.4 ppm compared with the observed δ of −68.1, −74.5, and −90.2 for T1, T3, and T2, respectively. The correlation of Sherriff and Grundy (1988) predicts chemical shifts of −74.4 to −75.1 ppm for the [4]Si sites, and not in the correct order. Incorporation of the bond-polarizability term (Eqs. 3, 4 of Sherriff and Grundy, 1988) produces a good linear correlation (r^2 = 0.96 for three data points), but the best-fit correlation constants are an order of magnitude different from those derived for all other [4]Si sites. The failure of these empirical correlations for garnet is probably not due solely to the presence of [6]Si, because Stebbins and Kanzaki (1991) obtained good results applying them to [6]Si chemical shifts, including the [6]Si site of En_{100} garnet.

Most of the spread of [4]Si δ for $MgSiO_3$ garnet is clearly related to the substitution of Si for Mg on the NNN octahedral sites. The amount of change per substitution of [6]Si for [6]Mg NNN, however, increases with each successive substitution, from 2.6 ppm between T(4Mg) and T(3Mg1Si) to 7.4 ppm between T(1Mg3Si) and T(4Si). This nonlinear change of δ with NNN substitution is surprising, because similar substitutions of tetrahedral Si for Al NNN in framework aluminosilicates produce a constant difference of about 5 ppm between the T[(n)Al] and T[(n − 1)Al] peaks for n = 1–4 (e.g., Ramdas and Klinowski, 1984).

These changes in ^{29}Si chemical shift with [6]Si for [6]Mg NNN substitution do follow closely the pairwise additivity model developed to predict substituent effects on chemical shifts in solution NMR studies (Vladimiroff and Malinowski, 1967; Kidd and Truax, 1968; Kidd and Spinney, 1973). The pairwise additive model is second order in the sense that the contribution to δ from one substituent group depends on the other substituents. This interaction of substituents is quantified empirically by assigning relative shifts of δ to adjacent pairs of substituent groups rather than to the individual substituents. In contrast, the more familiar case of Si substitution for Al in framework aluminosilicates can be described as directly additive (first order): the effects of the NNN on the ^{29}Si chemical shifts are independent of the other NNN sites, and the relative shift of δ is, thus, directly proportional to the number of NNN [4]Al atoms.

For the pairwise additivity model, determination of δ with NNN substitution around a fourfold-coordinated atom requires assignment of a relative shift for each type of tetrahedral edge (indexed by its bounding corners) and then summation of the pairwise shifts corresponding to the six edges of the tetrahedron to produce δ for that particular configuration. In En_{100} the tetrahedral Si have three possible combinations of octahedral NNN cation pairs (edges): Si-Si, Mg-Si, and Mg-Mg. Each of these adjacent NNN pairs contributes to [4]Si δ an amount denoted by η: $\eta_{Mg\text{-}Mg}$, $\eta_{Mg\text{-}Si}$, and $\eta_{Si\text{-}Si}$. For example, $\eta_{Si\text{-}Si}$ is the contribution to δ from tetrahedral edges having both of their O atoms bonded to [6]Si. For the T(4Si) site, δ is given by $6\eta_{Si\text{-}Si}$, whereas for T(2Mg2Si) it is $\eta_{Si\text{-}Si} + \eta_{Mg\text{-}Mg} + 4\eta_{Mg\text{-}Si}$.

To determine the pairwise shift constants for En_{100}, we define $\eta_{Mg\text{-}Mg} \equiv 0$ [origin set to the position of the T(4Mg) peak] and fit the appropriate sums of the two remaining

constants, $\eta_{Mg\text{-}Si}$ and $\eta_{Si\text{-}Si}$, to the observed δ using a least-squares method. The best-fit values are $\eta_{Si\text{-}Si} = -3.4$ ppm and $\eta_{Mg\text{-}Si} = -0.8$ ppm. These values reproduce the observed shifts to within ± 0.3 ppm. For the chemical shift of the T(1Mg 3Si) sites, we used the weighted average (-80.7 ppm). For the chemical shift of the T(0MG 4Si) site, we used the position of the smaller peak, -88.5 ppm, because this also appears to be the position of the peak due to T(4Si) sites in the $En_{80}Py_{20}$ sample. The shift of the peak for the crystallographic T2 site in En_{100}, T2(4Si), from that of the T(4Si) site in the cubic $En_{80}Py_{20}$ sample is due probably to the tetragonal structural distortion. For sites with more Mg NNN, δ appears to be less sensitive to the structural distortion. For example, δ for T(4Mg) is the same for En_{100} and $En_{80}Py_{20}$.

The pairwise additivity rule appears to account successfully for the variation of ^{29}Si δ with NNN octahedral cation substitution, and we use it empirically (see below) to estimate δ for all possible $^{[4]}Si$ sites in the intermediate composition garnets. However, the problem of understanding why the substitution effect on δ in En_{100} garnet is second order (pairwise), whereas in framework aluminosilicates it is first order, remains. The quantum-chemical explanation for pairwise additivity of δ (Vladimiroff and Malinowski, 1967) is that the electronic structure of one substituent group is modified by each of the neighboring substituent groups. This interaction ultimately modifies the substituent group's effect on the electronic structure of the atom of interest, on which its nuclear resonance frequency depends. Vladimiroff and Malinowski (1967) argue that substituent effects on δ should in general add pairwise, although direct additivity might be observed when substitution occurs far from the atom of interest. Consequently, most reports of pairwise additivity are for first-neighbor substitutions (e.g., ^{13}C δ for halogen-substituted methane), although some studies have reported second-neighbor pairwise additivity (e.g., ^{19}F δ in FC*XYZ*, *X*, *Y*, *Z* = H, F, Cl, Br, CN compounds).

However, because the $^{[4]}Si$-NNN and NNN-NNN distances are similar for the En_{100} garnet and tetrahedral frameworks, these distances cannot explain the contrasting chemical shift behavior of these structures. The $^{[4]}Si$-*M*, *M* = $^{[6]}Si$, or $^{[6]}Mg$ distance in En_{100} garnet (3.15–3.26 Å; Angel et al., 1989) falls in the range of T-T distances in tetrahedral frameworks (ca. 3.1–3.3 Å; e.g., Ramdas and Klinowski, 1984), and the distance between the NNN cations around the same $^{[4]}Si$ is 5.0 Å in En_{100} garnet and typically 4.5–5.5 Å in tetrahedral frameworks. A possible cause for the contrasting substituent effects on δ is the difference in flexibility of $^{[4]}Si$-O-NNN angles for the two structure types. Tetrahedral frameworks are somewhat flexible locally about the T-O-T linkages, whereas $^{[4]}Si$-O-$^{[4]}M$ in garnet may be more rigid because each tetrahedron and pairs of octahedra share edges with a common eightfold-coordinated Mg polyhedron. Additional observations of the pairwise effect in solid silicates are required, however, before any generalizations can be made.

$En_{80}Py_{20}$ and $En_{50}Py_{50}$ garnets

The spectra of the $En_{80}Py_{20}$ and $En_{50}Py_{50}$ garnet samples contain only six peaks or shoulders, but the crystals may have up to 15 local $^{[4]}Si$ sites. As a result, these spectra cannot be fitted to obtain directly the populations of the local $^{[4]}Si$ sites. However, by combining the approximate chemical shifts for each of the local $^{[4]}Si$ environments computed from the pairwise additivity model described above with intensities calculated assuming a random Mg,Al,Si distribution on the octahedral sites, we are able to reproduce the major features of these spectra. This result is consistent with the presence of little short-range Mg,Al,Si order on the octahedral sites.

Our XRD results show that the $En_{80}Py_{20}$ and $En_{50}Py_{50}$ samples have cubic symmetry, indicating that they contain no long-range order of the octahedral cations. Cubic garnets have only one tetrahedral site and one octahedral site in their average structure. Because the octahedral sites contain Mg, Al, and Si, there are 15 possible configurations of these cations about $^{[4]}Si$ (Table 3), compared with only five for each tetrahedral site in En_{100} garnet. Each of these 15 local $^{[4]}Si$ sites may, in principle, produce a separate peak.

We can estimate the chemical shifts of these 15 peaks with the pairwise additivity model, assuming that one set of pairwise chemical shift parameters describes the entire En-Py series. The agreement of the observed positions of the major peaks in the spectra of the $En_{80}Py_{20}$ and En_{100} samples supports this assumption. The spectrum of the $En_{80}Py_{20}$ sample (Fig. 2) is dominated by peaks at about -68, -71, -75, and -81 ppm, the same positions as the peaks assigned to T(4Mg 0Si), T(3Mg 1Si), T(2Mg 2Si), and T(1Mg 3Si) sites in the En_{100} sample. These sites are among the more probable Si environments in $En_{80}Py_{20}$, on the basis of a random distribution (Table 3). In contrast, several of the main peaks for the $En_{50}Py_{50}$ sample do not correspond to these chemical shifts, which is consistent with the required presence of more $^{[6]}Al$ NNN to the $^{[4]}Si$. For example, the shoulder at -69 ppm and the main peak at -73 ppm fall between peaks present in the more En-rich samples.

Application of the pairwise chemical shift model to the intermediate compositions requires pairwise shift parameters for the tetrahedral edges Al-Al, Al-Si, and Mg-Al in addition to those for Mg-Si, Mg-Mg, and Si-Si determined above for the En_{100} sample. The value for $\eta_{Al\text{-}Al}$ we obtain from the ^{29}Si chemical shift of pyrope, -72 ppm, giving $\eta_{Al\text{-}Al} = -0.66$ ppm. We estimate the two remaining parameters by assigning in the spectrum of the $En_{50}Py_{50}$ sample the peak at -83.5 ppm to T(1Al 3Si) environments, and the shoulder at -68.7 ppm to T(3Mg 1Al). With the previously determined pairwise shift constants, these assignments give $\eta_{Al\text{-}Si} = -1.75$ ppm and $\eta_{Mg\text{-}Al} = -0.2$ ppm, respectively. These estimates for the pairwise shift parameters agree with the generally accepted principle that the chemical shift for $^{[4]}Si$ should decrease with

substitution of [6]Al for [6]Mg NNN ($\eta_{Mg\text{-}Mg} > \eta_{Mg\text{-}Al}$ and $\eta_{Mg\text{-}Si} > \eta_{Al\text{-}Si}$) and increase with [6]Al for [6]Si substitution ($\eta_{Si\text{-}Si} < \eta_{Al\text{-}Si}$ and $\eta_{Mg\text{-}Si} < \eta_{Mg\text{-}Al}$).

We simulate the spectra of the $En_{50}Py_{50}$ and $En_{80}Py_{20}$ samples (Fig. 4) with 13 and 11 Gaussian curves, respectively. These peaks are centered at the chemical shifts calculated from the six pairwise chemical shift parameters (Table 3). We include no peaks for sites having fractional populations less than 0.01 for a random distribution, and sites with chemical shifts within 0.5 ppm of each other are represented as one peak. The widths of the peaks are fixed at values that increase monotonically from 1.1 ppm to 3.2 ppm with increasingly negative chemical shift. These widths are consistent with the results of unconstrained least-squares fits to these spectra. The simulations shown in Figure 4 were obtained by using initial intensities that correspond to those of a random distribution and allowing only the intensities to vary during minimization of the residuals. Unconstrained least-squares fits that produce residuals of a magnitude similar to those in these simulations (11–13 variable parameters) require full variation of seven curves (21 parameters) and unrealistic peak widths.

The simulations give good fits to the spectra with intensities for individual peaks that differ from those of a random distribution by no more than ± 0.03 for $En_{50}Py_{50}$ and ± 0.05 for $En_{80}Py_{20}$. Small changes in the constrained peak positions (ca. 0.5 ppm) and widths can change the fitted intensities by as much as ± 0.03. Even with such variation, however, the relative intensities of the main regions of the spectra (i.e., sums of individual peaks that correspond to the main peaks and shoulders in the observed spectra) remain constant and differ insignificantly from those of a random distribution. The fitted intensities that differ most from a random distribution occur as adjacent pairs, in which one is more and the other less intense than for a random distribution. For example, for $En_{80}Py_{20}$ the fitted intensity for T(3Mg 1Si) + T(1Mg 3Al) is greater than for a random distribution (+0.05), and the intensity of the adjacent peak, due to T(2Mg 1Al 1Si) + T(4Al), is smaller than for a random distribution (−0.06).

We conclude from these results that the ^{29}Si NMR spectra are compatible with the existence of little short-range order of the octahedral cations, and in particular there is no evidence of residual majorite-like or pyrope-like order in the intermediate compositions. A majorite-like ordering scheme would produce greater intensities for the T(4Si) and T(4Mg) peaks than a random distribution. Both of these peaks are fairly well resolved, and the fitted intensities are very similar to those of random distribution. The fitted intensity of the T(4Si) peak for $En_{80}Py_{20}$ is, in fact, smaller than that calculated for a random distribution. An additional concentration of pyrope-like T(4Al) environments would produce increased intensity at −72 ppm, which is not observed. Also, the composition of the $En_{50}Py_{50}$ sample could be satisfied by complete ordering onto T(Mg 2Al Si) sites, but the fitted intensity for this site is also close to that of a random distribution.

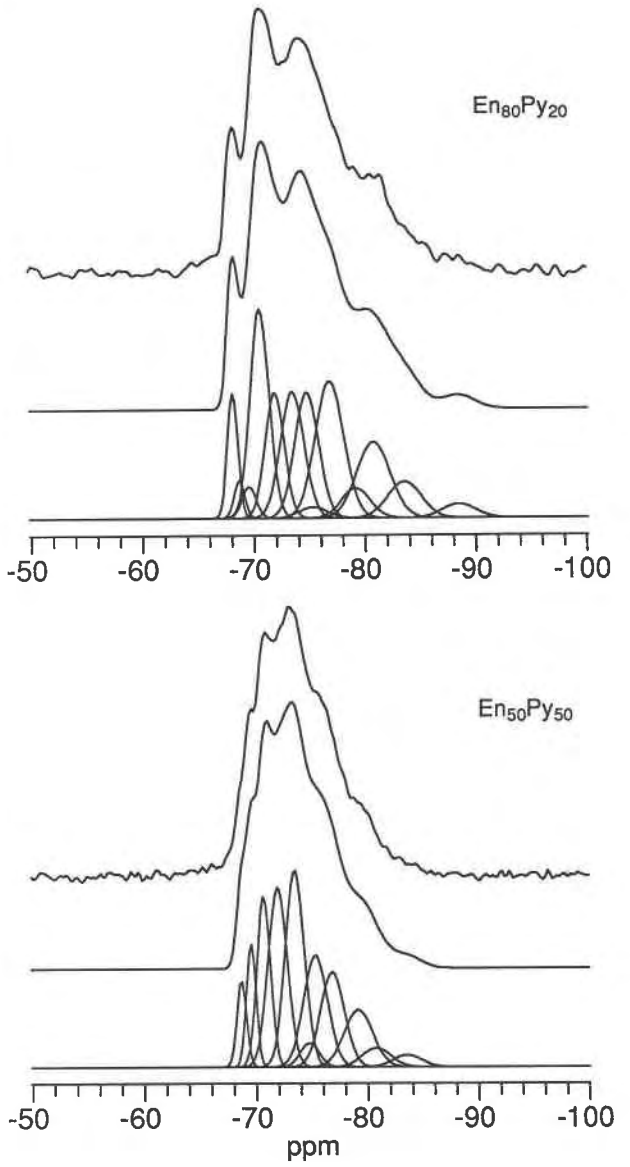

Fig. 4. Simulations of ^{29}Si NMR spectra of the $En_{80}Py_{20}$ and $En_{50}Py_{50}$ samples. Observed spectra are at the top. Simulations (middle) are a sum of the Gaussian curves shown at the bottom of each set. Only the peak intensities were varied in the fitting procedure. Peak positions and widths were obtained independently and fixed in the simulations. See text for details.

Unfortunately, even with these apparently reasonable estimates for the chemical shifts and peak widths, all the peaks other than those at the edges of the spectra overlap significantly, and it is not possible to determine precisely the degree of short-range order on the octahedral sites. The most that we can say based on the NMR spectra is that the extent of short-range order in the $En_{80}Py_{20}$ and

$En_{50}Py_{50}$ samples appears to be small and is certainly much less than that in the end-member En_{100} sample.

Acknowledgments

This research was supported by NSF grants EAR-9004260 to R.J.K. and EAR-9003748 to T.G. We wish to thank Ian Steele for the electron microprobe analysis of the garnet and Eric Oldfield for discussions on chemical shifts. Ross Angel and Jonathan Stebbins provided helpful critical reviews. We also thank the University of Illinois Laboratory for Supercomputing in Hydrology for computing facilities and Jay D. Bass for use of the pyrope sample.

References cited

Akaogi, M., and Akimoto, S. (1977) Pyroxene-garnet solid solution equilibria in the systems $Mg_4Si_4O_{12}$-$Mg_3Al_2Si_3O_{12}$ and $Fe_4Si_4O_{12}$-$Fe_3Al_2Si_3O_{12}$ at high pressures and temperatures. Physics of Earth and Planetary Interiors, 15, 90–104.

Akaogi, M., Navrotsky, A., Yagi, T., and Akimoto, S. (1987) Pyroxene-garnet transformation: Thermochemistry and elasticity of garnet solid solutions, and application to a pyrolite mantle. In M.H. Manghnani and Y. Syono, Eds., High-pressure research in mineral physics, Geophysical Monograph vol. 39, p. 209–219. American Geophysical Union, Washington, DC.

Angel, R.J., Finger, L.W., Hazen, R.M., Kanzaki, M., Weidner, D.J., Liebermann, R.C., and Veblen, D.R. (1989) Structure and twinning of single-crystal $MgSiO_3$ garnet synthesized at 17 GPa and 1800 °C. American Mineralogist, 74, 509–512.

Dupree, R., Lewis, M.H., and Smith, M.E. (1988) Structural characterization of ceramic phases with high-resolution ^{27}Al NMR. Journal of Applied Crystallography, 21, 109–116.

Grimmer, A.R., von Lampe, F., and Mägi, M. (1986) Solid-state high-resolution ^{29}Si MAS NMR of silicates with sixfold coordinated silicon. Chemical Physics Letters, 132, 549–553.

Hatch, D.M., and Ghose, S. (1989) Symmetry analysis of the phase transition and twinning in $MgSiO_3$ garnet: Implications to mantle mineralogy. American Mineralogist, 74, 1221–1224.

Janes, N., and Oldfield, E. (1985) Prediction of silicon-29 nuclear magnetic resonance chemical shifts using a group electronegativity approach: Applications to silicate and aluminosilicate structures. Journal of the American Chemical Society, 107, 6769–6775.

Kato, T., and Kumazawa, M. (1985) Garnet phase of $MgSiO_3$ filling the pyroxene-ilmenite gap at very high temperature. Nature, 316, 803–805.

Kidd, R.G., and Spinney, H.G. (1973) Germanium-73 nuclear magnetic resonance spectra of germanium tetrahalides. Journal of the American Chemical Society, 95, 88–90.

Kidd, R.G., and Truax, D.R. (1968) The occurrence of mixed tetrahaloaluminate ions shown by aluminum-27 nuclear magnetic resonance spectroscopy. Journal of the American Chemical Society, 90, 6867–6869.

Kirkpatrick, R.J., Howell, D., Phillips, B.L., Cong, X.-D., Ito, E., and Navrotsky, A. (1991) MAS NMR spectroscopic study of $Mg^{29}SiO_3$ with the perovskite structure. American Mineralogist, 76, 673–676.

McMillan, P., Akaogi, M., Ohtani, E., Williams, Q., Nieman, R., and Sato, R. (1989) Cation disorder in garnets along the $Mg_3Al_2Si_3O_{12}$-$Mg_4Si_4O_{12}$ join: An infrared, Raman and NMR study. Physics and Chemistry of Minerals, 16, 428–435.

O'Neill, B., Bass, J.D., Rossman, G.R., Geiger, C.A., and Langer, K. (1991) Elastic properties of pyrope. Physics and Chemistry of Minerals, 17, 617–621.

Press, W.H., Flannery, B.P., Teukolsky, S.A., and Vetterling, W.T. (1986) Numerical recipes: The art of scientific computing. Cambridge University Press, Cambridge, U.K.

Ramdas, R., and Klinowski, J. (1984) A simple correlation between isotropic ^{29}Si-NMR chemical shifts and T-O-T angles in zeolite frameworks. Nature, 308, 521–523.

Remsberg, A.R., Boland, J.N., Gasparik, T., and Liebermann, R.C. (1988) Mechanism of the olivine-spinel transformation in Co_2SiO_4. Physics and Chemistry of Minerals, 15, 498–506.

Sawamoto, H. (1987) Phase diagram of $MgSiO_3$ at pressures up to 24 GPa and temperatures up to 2200 °C: Phase stability and properties of tetragonal garnet. In M.H. Manghnani and Y. Syono, Eds., High-pressure research in mineral physics, Geophysical Monograph, vol. 39, p. 209–219. American Geophysical Union, Washington, DC.

Sherriff, B.L., and Grundy, H.D. (1988) Calculations of ^{29}Si MAS NMR chemical shift from silicate mineral structure. Nature, 332, 819–822.

Smith, J.V., and Blackwell, C.S. (1983) Nuclear magnetic resonance of silica polymorphs. Nature, 303, 223–225.

Smith, K.A., Kirkpatrick, R.J., Oldfield, E., and Henderson, D.M. (1983) A ^{29}Si MAS NMR spectroscopic study of rock-forming silicates. American Mineralogist, 68, 1206–1215.

Stebbins, J.F., and Kanzaki, M. (1991) Local structure and chemical shifts for six-coordinated silicon in high-pressure mantle phases. Science, 251, 294–298.

Vladimiroff, T., and Malinowski, E.R. (1967) Substituent effects. VI. Theoretical interpretation of additivity rules of NMR using McWeeny group functions. Journal of Chemical Physics, 46, 1830–1841.

Manuscript received July 1, 1991
Manuscript accepted March 20, 1992